



Stability of mesoscale vortex under sea ice friction in the Arctic

BY MAX COPPIN, SUPERVISED BY XAVIER CARTON¹ and CAMILLE LIQUE¹
¹Univ. Brest, CNRS, IRD, Ifremer, Laboratoire d'Océanographie Physique et Spatiale (LOPS), IUEM, Brest, France

Abstract

The effects of upper lid friction on the stability, merging, and propagation of power exponential shielded vortices are investigated in a two-and-a-half-layer shallow water model. The reduced gravity approximation is applied for an Arctic Ocean's idealized stratification. The results obtained numerically by a pseudo-spectral code are that friction acts as a catalyst for breaking, as it primarily affects the core of the vortex by attenuating its vorticity. Thus the action of the annulus deforms the core further than in ice-free conditions without modifying the preferred instability of cyclones versus anticyclones. Coalescence is only delayed under sea-ice drag and the trajectory of opposite-sign dipole is curved in respect of the free ice conditions. In conclusion, sea-ice friction reduces the lifetime of the vortices and increases the merging time beyond the Ekman layer and the mixed layer. We can therefore expect a change in the rheology of the ice to modify the resilience of the eddies and the fluxes associated with them.

Keywords: Arctic Ocean; Sea-ice friction; Vortex; Stability; Sea-ice interactions

1. Introduction

Eddy structures are ubiquitous in all oceans and have been shown to be abundant. However, one part of the Arctic Ocean has the particularity, like the Southern Ocean, of having a sea ice cover, with a complex seasonality and rheology. There is no doubt that the presence of this sea ice cover interacts with the ocean, mechanically as an additional source of friction and through the deformation of the ice by the ocean, and thermodynamically through the exchange of heat and salt fluxes. It thus directly modifies the water masses of the Arctic Ocean. From a dynamic point of view, in the Arctic Basin, observations made under the sea ice [Marcinko et al., 2015] [von Appen et al., 2022] and results from very high resolution idealized numerical simulations

[Mensa and Timmermans, 2017] suggest that the mesoscale energy in ice-covered regions is relatively low compared to the ocean dynamics characteristic of ice-free regions. This suggests that, at first order, the mesoscale activity may be fundamentally different in the presence of sea ice.

Nevertheless, eddies are not absent from these regions, as shown by observations [Newton et al., 1974, Manley and Hunkins, 1985, D'Asaro, 1988, Carpenter and Timmermans, 2012, Zhao and Timmermans, 2015, Pnyushkov et al., 2018, Timmermans et al., 2008, Zhao et al., 2014, 2016, Johannessen et al., 1987]. The typical scale of the vortices captured by these observations are about the size of the Rossby radius of deformation ($\sim 10\text{km}$). They are centered at depth between 50–200 m, with a vertical extension between 30 and 150m, and they have a typical radial velocity of $10\text{--}30\text{cm}\cdot\text{s}^{-1}$, and a lifetime longer than 6 months. Some observations Newton et al. [1974], Manley and Hunkins [1985], Timmermans et al. [2008] have revealed a disparity between the number of cyclones and anticyclones, with an approximate 95% dominance of anticyclones and with a general size superior than the cyclones. Several hypotheses may explain this:

- A bias in the detection method that would favor the detection of eddies with one polarity over the other.
- The generation of these eddies would favor anticyclones rather than cyclones. Manucharyan and Timmermans [2013], Chao and Shaw [1996], Brannigan et al. [2017] have examined a mechanism described by Spall [1995] to the Arctic Ocean case, which suggests that frontal instabilities generate a baroclinic dipole of opposite sign that propagates over large distances. The upper-layer eddy is preferentially a weaker cyclone than the lower-layer anticyclone. The top layer cyclone would be dissipated by the drag of the ice, and the lower anticyclone would be preserved [Chao and Shaw, 1996].
- The dissipation and the stability of the vortex in this region could also favor one type of vortex, by dissipating preferentially cyclones.

The stability of an eddy forced by ice friction is still not well understood. Firstly the stress at the interface between sea-ice and ocean is too complex to well represent the space-time variation of the drag. Secondly, the parameterization of this stress in models is set for a given rheology by adding a drag coefficient that makes it imprecise.

The Arctic Ocean, even more than the others, is subject to the effects of climate change. The maximum ice coverage of the Arctic Ocean is decreasing of $12.7\%\pm 2\%$ each decade since 1980 [Meier and Stroeve, 2022], and the ice pack tends to become younger in areas where the ice was multi-year old while the MIZ is expanding. All these parameters influence the ice properties and thus the forcing between the ice and the ocean and especially the friction.

Depending on the intensity of the drag (for a vortex at a given depth) the life-time and thus the pathway of the vortex can be greatly shortened or enhanced. Based on the analysis of the AIDJEX project data that took place over 1974–1985 in the Canadian Basin combined with a theoretical scaling, Ou and Gordon [1986] has quantified the expected spindown of a vortex in

response to the sea ice drag. Our study aims to expand their work by exploring a wider range of linear friction with a different stratification to take into account the changes affecting the Arctic Ocean climatology [Rosenblum et al., 2022]. This study will also not be restrained to the mesoscale, but we will also consider submesoscale eddies.

This report is structured as follows: section 2 describes the physical and numerical models used to investigate the linear and non linear stability of a perturbed vortex. In section 3 we describe the effects of friction on the linear stability and its finite amplitude evolution. In section 4, we explore the interaction between vortices under upper lid friction. We discuss the results in section 5.

2. Model and physical settings

2.1. Two-and-a-half-layer shallow water model

We want to examine the effects of sea-ice friction on the dynamics of the vortices in the Arctic Ocean. To do so the sensitivity of the stability, the coalescence, and the propagation processes to different drags are good indicators. As mentioned before, previous work has shown that the generation of instabilities under sea ice may lead to the formation of a baroclinic pair of vortices [Manucharyan and Timmermans, 2013] but with the top vortex decaying rapidly [Ou and Gordon, 1986]. That is why a two-and-a-half-layer model is suitable to capture the complexity of the real Arctic small scale structures while maintaining a degree of idealization. In addition, we choose to base our analysis on the shallow water equations in order to be able to examine if there is an asymmetry between Cyclones and Anticyclones in their response to the effects of sea ice friction.

The two-and-a-half-layer shallow water equations, with uniform background rotation, a frictional rigid lid, are written in polar coordinate:

$$\left[\partial_t + u_i \partial_r + \frac{v_i}{r} \partial_\theta \right] u_i - \frac{v_i^2}{r} - v_i f_0 = -g'_2 \partial_r(\eta_2) + \delta_{i,1} (-g'_1 \partial_r(\eta_1) - C_d u_1) \quad (1)$$

$$\left[\partial_t + u_i \partial_r + \frac{v_i}{r} \partial_\theta \right] v_i + \frac{u_i v_i}{r} + u_i f_0 = -\frac{g'_2}{r} \partial_\theta(\eta_2) + \delta_{i,1} \left(-\frac{g'_1}{r} \partial_\theta(\eta_1) - C_d v_1 \right) \quad (2)$$

$$\left[\partial_t + u_i \partial_r + \frac{v_i}{r} \partial_\theta \right] (H_i + \delta\eta_i) + \frac{(H_i + \delta\eta_i)}{r} [\partial_r(ru_i) + \partial_\theta(v_i)] = 0 \quad (3)$$

where (u_i, v_i) are the (radial, azimuthal) velocity, H_i the depth and η_i the elevation of the interface between the i th and the $(i+1)$ th layers (counted from the top), $\delta\eta_i$ is the thickness anomaly in layer i , $\delta_{i,1}$ the Kronecker delta, g'_i the reduced gravity, C_d the drag coefficient for a linear friction.

The detailed adimensional equations are given in the appendix.

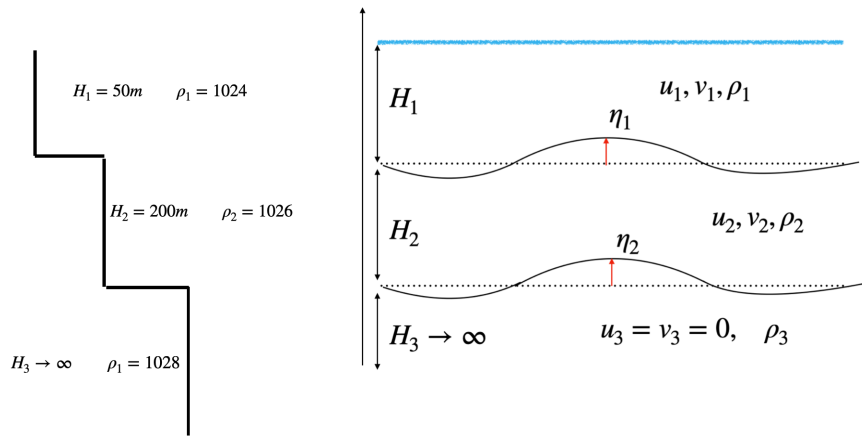


Figure 1: Idealisation of the Arctic ocean stratification into a two-and-a-half-layer system

2.2. Idealized vortex in the Arctic Ocean

Figure 1 shows the idealized stratification for the Arctic Ocean in two finite and one infinite layer from the data used by Rosenblum et al. [2022], Newton et al. [1974]. The first layer starting from the top represents the mixed layer in which we consider no mean flow. The vortices are contained in the second layer and thus interact with the other layers by deflecting the interfaces.

The vortices we consider are axisymmetric with a power exponential profile. They are surrounded by a ring of opposite-sign vorticity. Those kinds of vortices are called shielded vortices [Carton, 2001], and their velocity can be expressed as:

$$V(r) = V_0 \frac{r}{R} \exp\left(\left(\frac{-r}{R}\right)^\alpha\right)$$

The parameters α is the steepness of the profile, the larger α is, the steeper the vorticity gradient is, meaning that α provides the frontality of the vorticity. This frontality in the Arctic Ocean is only little constrained from observations, hence we will set by default the steepness to $\alpha = 2$ or $\alpha = 3$ for our study. That steepness is common and often observes in other oceans. All the characteristics and adimensional numbers describing the characteristics of the vortices considered in our analysis are given in Table 2

2.3. Representation of the presence of sea ice

In our study, we are only interested in the frictional impact of sea ice. Thus, we represent it by a rigid lid above the first layer inducing a frictional forcing. The drag coefficient corresponding to the pack ice has been chosen according to the literature [Mazloff et al., 2010] [Cole et al., 2014] [Pease et al., 1983]. The drag $C_d \in [2 - 8e - 3]$ is the quadratic coefficient of friction. However, the model we use only allow linear drag. Hence, we make the following approximation in our model:

$$F = C_d |\bar{u}| u \iff F = C_d^* u$$

Vortex's parameter and setting		
	Idealised Conditions	Adimensional
Radius	7km	0.5
Coriolis parameter f	$1.4 \times 10^{-4} s^{-1}$	1
Rossby deformation radius	12km	0.86
Rotation rate Ω	$4.2 \times 10^{-5} s^{-1}$	0.3
Rossby number	0.3	0.1 – 1
Burger number	3.14	3.1
$H1$	50m	0.2
$H2$	200m	0.8
Reduced gravity g'_1	0.0095	0.7
Reduced gravity g'_2	0.0286	1.6

Figure 2: Real condition parameters based on the conditions observed during the Aidjex project [Newton et al., 1974]. And corresponding adimensional values.

With $C_d^* = C_d |\bar{u}|$ and F the friction

2.4. Non linear model implementation and initial condition

We resolve this system using a pseudo-spectral code in a biperiodic square domain of 128 nodes in each direction. Two layers are implemented with respectively a depth of 1/5 and 4/5 of total height for the top and lower layer to represent the vertical distribution given in Table 2. A rigid lid is set only on top of the first layer. The fast waves are filtered out by an Asselin Filter. The numerical stability is reached with the minimum biharmonic viscosity.

The mean flow is an isolated circular vortex in layer 2 respecting the following conditions:

$$\bar{u}_1 = 0; \quad \bar{u}_2 = 0$$

$$\bar{v}_1 = \kappa v_2; \quad \bar{v}_2 = V_0 \frac{r}{R} \exp(-(\frac{r}{R})^\alpha)$$

With R the vortex radius, (u_i, v_i) are the (radial, azimuthal) velocity of the i th layer. If $\kappa \neq 0$, the top layer is not at rest and the vortex become barocline.

The velocity and the pressure gradient are in cyclogeostrophic balance given by:

$$\frac{\bar{v}^2}{r} + f_0 \bar{v} = g \frac{1}{\rho_0} \frac{dp'}{dr} \quad (4)$$

The Cyclone and the Anticyclone are set by an inversion of the vorticity sign, and the initial elevation η is computed from the cyclogeostrophic balance.

We further investigate the effect of ice drag on the general stability and spin down by varying the drag coefficient C_d and the its influence on flow with different velocity and dynamical scale by varying the Rossby number Ro .

3. Stability of a vortex in conditions similar to the Arctic Ocean

3.1. Vortex's stability in ice-free conditions

In this section, we examine the stability condition of a shielded vortex with a steepness $\alpha = 3$ in the second layer of our model, without friction exerted on the upper lid and the first layer is at rest. This corresponds to examination of the stability of a vortex in ice-free condition.

We verify the Ripa's general stability conditions for a multi-layer model with an axisymmetric flow [Ripa, 1991].

If at least one of the condition below is not satisfied, the vortex is unstable barotropically or baroclinically.

First condition

$$\exists \omega \quad \forall r, \quad \frac{\Omega_i(r) - \omega}{dq_i/dr} > 0 \quad (5)$$

Second condition

$$\exists \omega \quad \forall r, \quad g_2'^2 < (g_1' + g_2' - \gamma_1(r))(g_2' - \gamma_2(r)) \quad \text{With } \gamma_i(r) = \frac{(\Omega_i(r) - \omega)^2}{H_i} \quad (6)$$

With $\Omega(r) = V(r)/r$ and q_i the potential vorticity of the i th-layer,

Given that the vorticity profile of the vortices under study is exponential in power, if $\alpha > 1$ then the derivative of the potential vorticity cancels out and changes sign. Thus the first condition is not respected. Indeed, dq_i/dr being in the denominator (this condition does not require to be defined over the whole domain) if $\Omega - \omega > 0$ then $\frac{\Omega - \omega}{dq_i/dr}$ changes sign over the domain, same thing if $\Omega - \omega < 0$.

If only one layer is considered, the sign inversion of the potential vorticity derivative shows the instability of the vortex with respect to the Fjortoft criterion and the Rayleigh criterion.

An other criterion described by Baey and Carton [2002], derived from Holton [2004] allows us to determine if the structure respects the inertial stability condition.

Inertial stability condition

$$(1 + Ro\frac{v_i}{r})(1 + Roq_i) < 0 \quad (7)$$

Numerically this criterion is not respected for $Ro > 0.5$

The relative importance of the baroclinic or the barotropic effects is correlated with the horizontal shear and the stratification. The barotropic instability will be more important in the case of a strong vorticity screen. In contrast, the baroclinic effects are enhanced in the presence of strong Burger numbers [Pedlosky, 1987]. Thus for the conditions considered here (Table 2) with a $Bu = 3.1$ and setting $\alpha = 3$, we expect the vortices to be destabilized dominantly through barotropic instability.

The inertial and centrifugal instabilities are more present in case of strong vorticity, and thus are more present at submesoscale (ageostrophic effect).

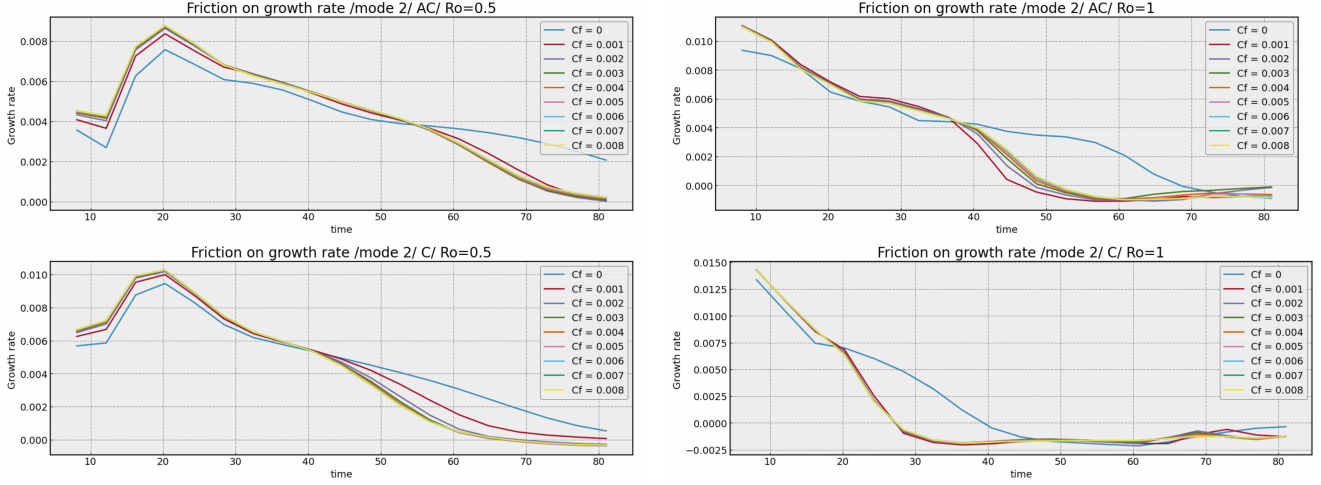


Figure 3: Evolution of the perturbation growth rate in time (in days) for different values of the upper lid friction on a cyclonic vortex (top panels), an anticyclonic vortex (lower panels) for $Ro = 0.5$ (left panels) and $Ro = 1$ (right panels)

3.2. Influence of an upper lid friction on the linear stability

Since the depth of the layer affected by friction boundary is greater than the Ekman depth which is about $20m$, we do not expect the vortex to be drastically slowed down. According to Pedlosky [1987], we rather expect an attenuation of the perturbation. However, Figure 3 shows the evolution of the perturbation growth rate for a cyclone and an anticyclone, for different Rossby numbers and values of the drag coefficient. We find that, for the $Ro = 0.5$ case, there is a peak of growth rate at the 20th day of simulation for both the anticyclone and cyclone. This peak corresponds to the time taken by the perturbation to find the normal mode of perturbation. We notice also for each graph the existence of two periods: a first one when the growth rate is larger for larger friction, and a second period when it is the opposite, and the friction acts against the perturbation in accordance with theory. In the second period, the evolution become non-linear and therefore cannot be diagnosed with linear stability analysis. The timing of the switch between the two regimes corresponds to the time when the curves of different friction intersect.

The amplification of perturbation by friction likely arises from the fact that friction primarily affects the central core of the vortex (see Figure 4). Regardless of the level of friction, the outer annulus remains almost unchanged; however, conversely, the vorticity of the core diminishes (in absolute terms) until a certain threshold is reached. For both cyclones and anticyclones, greater friction leads to a more rapid reduction in vorticity. This indicates that the core vorticity of the vortex will be more attenuated compared to its annulus. Consequently, friction intensifies the deformation caused by the annulus on the core, resulting in an accelerated initial period of deformation. As a result, the instability is enhanced by friction.

This can be understood easily by considering the equation of the rotational of the momentum

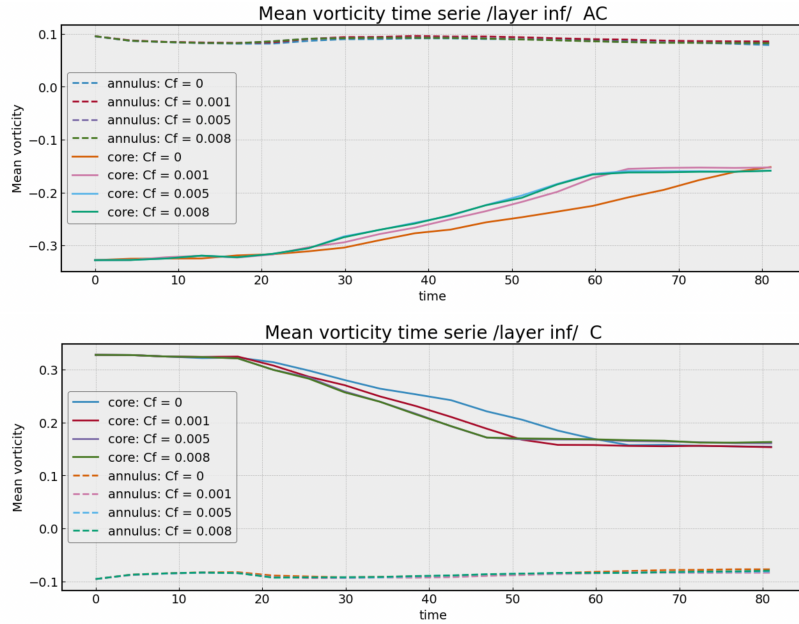


Figure 4: Evolution of the negative and positive relative vorticity budget in time (in days) for different values of upper lid friction on a cyclonic vortex (top panel), anticyclonic vortex (lower panel) for $Ro = 0.5$

equation in non rotative frame in a non-viscous fluid subject only to linear friction :

$$\frac{D\zeta}{Dt} = -C_d \zeta$$

With ζ the vorticity and C_d the linear coefficient of friction.

Thus the impact of friction is stronger for larger values of ζ , inducing a larger reduction of ζ .

Furthermore, when we compare the linear stability of a cyclone versus an anticyclone, we notice the growth rate is higher for the cyclone than for the anticyclone whatever the value of friction. That reveals that friction preserves asymmetry without accentuating or attenuating it. However, Figures 3 and 4 suggest an asymmetry in the length of the first period. It is longer for anticyclones than for cyclones, and this delay before the curves of different friction intersect for the cyclone and anticyclone is shortened for a larger Rossby numbers.

Figure 5 shows that, as the flow gets closer to the ageostrophic regime ($Ro \sim 1$), the frictional case diverges more significantly from ice-free conditions ($C_d = 0$). This is consistent with the dissipative nature of the sea-ice friction because it is a quadratic function of the velocity of the flow.

So far, we have seen that friction has a destabilizing effect on vortex in the first period and tends to increase the deformation of the vortex's core.

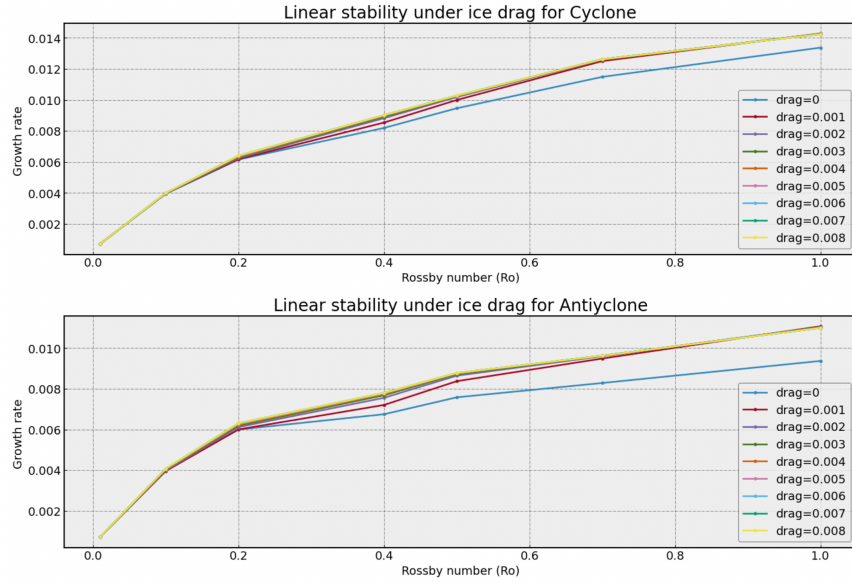


Figure 5: Growth rate of the perturbation as a function of the Rossby number for different values of upper lid friction on a cyclonic (top panel) and anticyclonic (lower panel) vortex

3.3. Influence of upper lid friction on finite amplitude stability of an elliptical perturbed circular vortex

We now analyze the influence of friction on the finite amplitude regime of the elliptical perturbation superimposed on the shielded vortex in a numerical model of the two-and-a-half layer SW equation. Two sets of experiments are performed, each one comparing frictionless conditions to conditions with an upper lid friction ($Cd = 5 \times 10^{-3} kg.s^{-1}$) for both a cyclone and an anticyclone. The first result is that the breaking of the vortices occurs much more rapidly in the case where friction is applied (Figures 6,7 and 8). In Figure 6, the breaking of the vortex is at day 81 whereas in the presence of friction, it happens earlier at day 59. For Figure 7 the breaking does not occur within the time-frame of the experiment for the ice-free condition but does happen on day 135 with upper-lid friction. We also notice, that this time interval between breaking is similar for the case of a frictionless cyclone (Figure 6 B) and for the case of upper-lid friction applied to an Anticyclone (Figure 7 A) and the instability process roughly the same. This is also true if we take $Ro = 1$ (case not represented for the anticyclone). Based on this, we can say friction does not affect differently depending on the cyclonic or anti-cyclonic nature of the vortex but preserves the more stable state of the anticyclone observed in ice-free conditions Carton [2001]. Hence, we can conclude that friction acts as a catalyst in the breaking of vortices, by speeding it. The processes at play for the breaking are similar to those described by Flierl [1988] and Carton and Mcwilliams [1989]. On Figure 7 B) Day 34: Under the influence of the perturbation of mode 2, the core and the annulus take two phased shifted elliptical shapes. On day 68, the perturbation rotates, enhances the deformation of the core, elongates it, and eventually breaks the annulus to form a tripole. On day 93, the extremity of the core ellipse and the tail of the two satellites are also elongated and form frontal structures.

On day 127, the core breaks into two dipoles and the front surge creating turbulence.

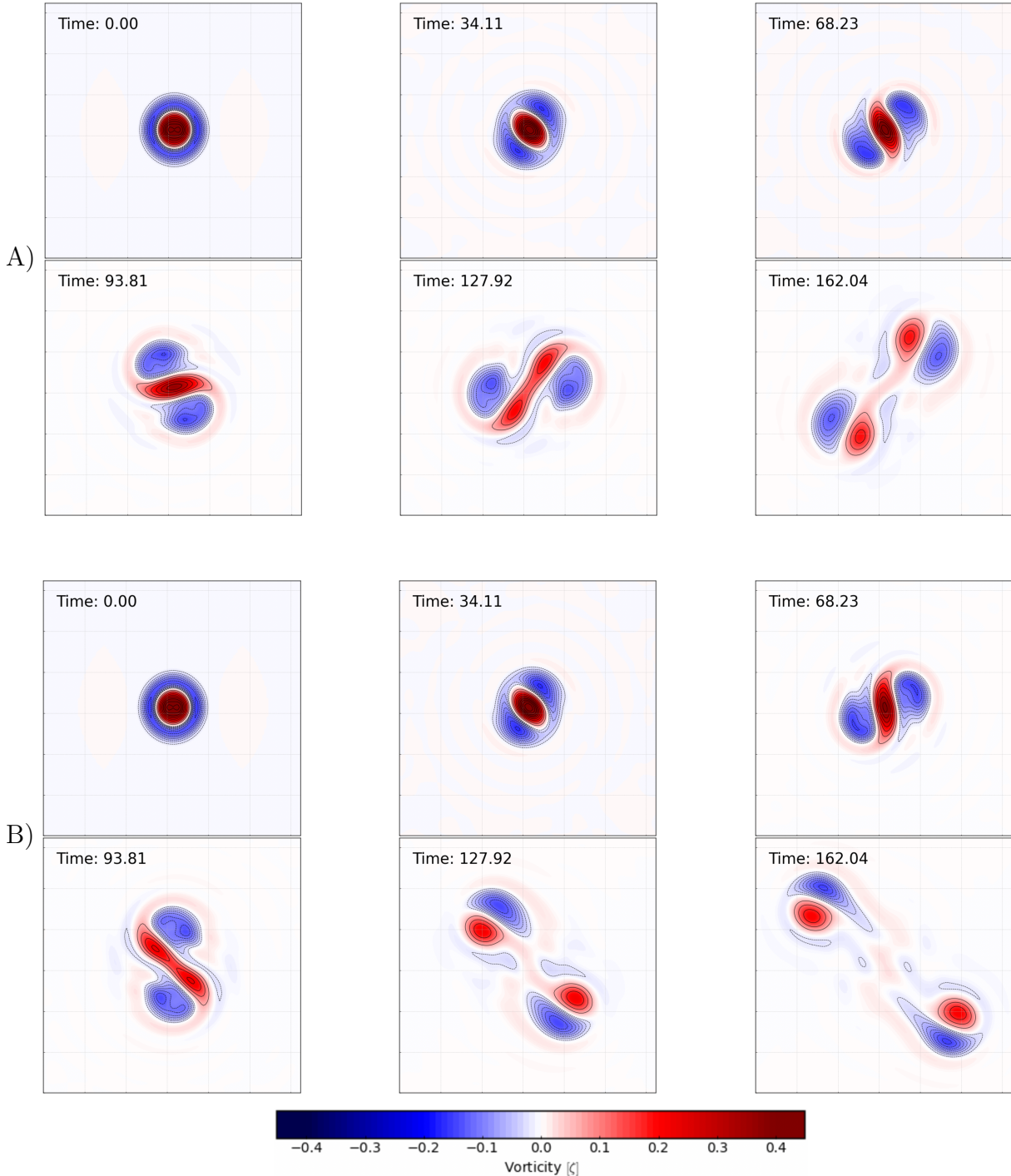


Figure 6: Time-evolution of relative vorticity showing unstable cyclonic vortex with a steepness $\alpha = 3$ in the lower layer with an $m = 2$ normal-mode (elliptical) perturbation, Rossby number $Ro = 0.5$, in an idealized Arctic stratification; $Bu = 3.1$. A): No friction on upper lid. B): Ice–ocean drag coefficient applied on upper lid $C_d = 5 \times 10^{-3}$. The time is in days

The deformation of the vortex's core is accentuated in the case with friction. This confirms

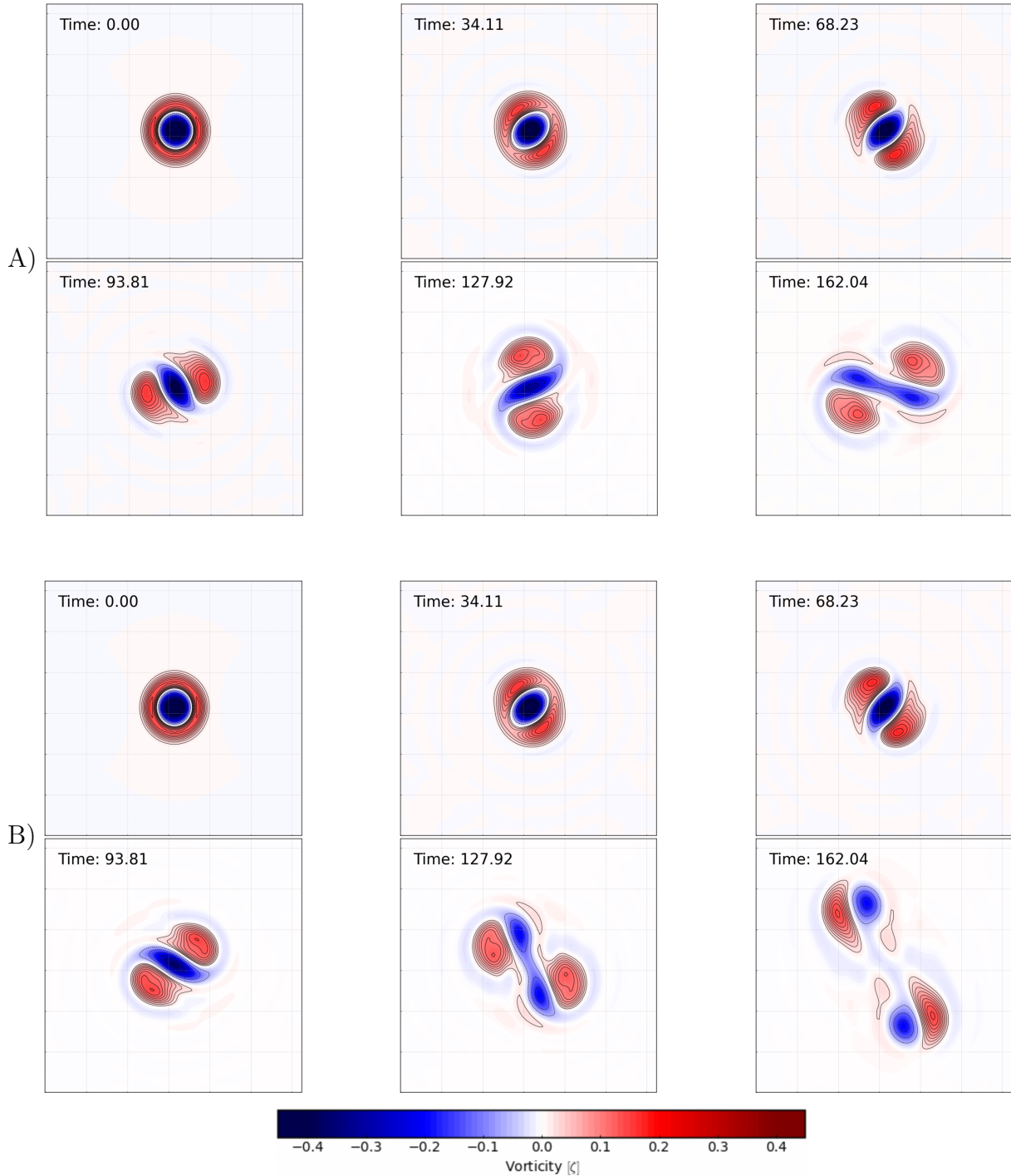


Figure 7: Time-evolution of relative vorticity showing unstable anticyclonic vortex with a steepness $\alpha = 3$ in the lower layer with an $m = 2$ normal-mode (elliptical) perturbation, Rossby number $Ro = 0.5$, in an idealized Arctic stratification; $Bu = 3.1$. A): No friction on upper lid. B): Ice–ocean drag coefficient applied on upper lid $C_d = 5 \times 10^{-3}$. The time is in days

the result from the linear stability analysis. The core is elongated (smaller aspect ratio) and therefore the vortex rotates more slowly than in friction-less experiments. It follows the behavior of the Kirchhoff Ellipse: [Carton, 2001]

$$\Omega(\lambda) = \frac{\omega_0 \lambda}{(1 + \lambda)^2}$$

With $\lambda = b/a$ the aspect ratio, a, b respectively the semi major (minor) axis, Ω the rotation of the ellipse, ω_0 the rotation of the vortex. This reduced rotation of the Kirchhoff Ellipse ensures that the dipoles remaining after the break have a higher speed than in the ice-free condition. This increase in velocity separates the two pairs quicker and thus reduces the time of filamentation between it.

At $Ro = 0.5$ the Anticyclonic evolution in the presence of friction (Figure 7 B) is similar and of the same order of magnitude and time as the friction-less case of the cyclonic (Figure 6 A). That shows that the Anticyclones are more stable than Cyclones.

The case of a the cyclonic vortex at $Ro = 1$ forced by friction is shown in Figure 8. After the breaking, the anticyclonic screen is wrapped around the core and thus leads to two smaller shielded vortices. To analyze it we perform a diagnostic on the strain and shear evolution within the vortex (Figure 9). For the cyclone, the deformation rate grows rapidly, which means the breaking is strong and thus the negative vorticity patches are therefore driven by the two parts of the core. As we shall see in the next section, friction has the effect of reducing the radius of curvature of the trajectory of dipoles of opposite signs. This rotational movement allows the annulus to reform.

In summary we have seen that friction acts as a catalyst in the breaking of vortices and ejects the residue of the breaking with a higher velocity.

4. Interaction of vortices under sea-ice

4.1. Like-sign Vortices under upper lid friction

Coalescence occurs when two similar-sign vortices are close enough to exchange fluid mass and then collapse into a single coherent structure. It has been shown Polvani et al. [1989], Griffiths and Hopfinger, Verron and Valcke [1994] that the distance between the two core's centers determines the merging or not of the vortices. Depending on this distance several cases may occur.

- The first one for close enough vortices and little or no antagonistic mechanism, is the merging case, as shown on Figure 10. On day 4 the two cores exchanges fluid masses and form an ellipse. After that, the ellipse rotates and the tails of the ellipse are stretching and form fronts. These are separate from the newly formed cores and surges. After one month the fusion gives a tripole which becomes stable. As underlined by Valcke and Verron [1997], the coalescence of vortices separated by a small distance as ($d = 0.8$; with d the distance between the centers corresponding to $d = 1.6R$ in table 2) leads to the formation of a tripole because the evolution of the merging is similar in the configuration

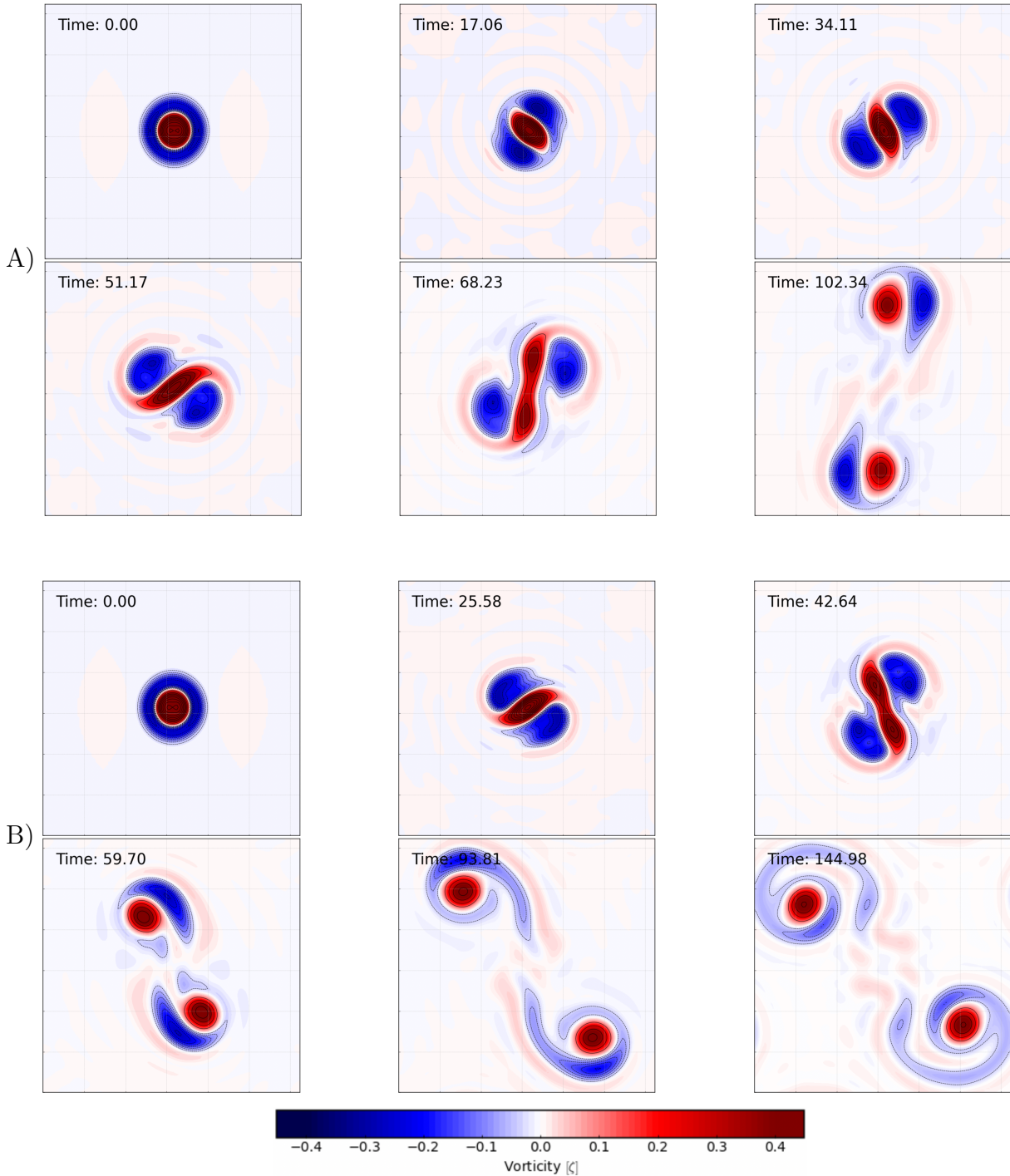


Figure 8: Time-evolution of relative vorticity showing unstable cyclonic vortex with a steepness $\alpha = 3$ in the lower layer with an $m = 2$ normal-mode (elliptical) perturbation, Rossby number $Ro = 1$, in an idealized Arctic stratification; $Bu = 3.1$. A): No friction on upper lid. B): Ice-ocean drag coefficient applied on upper lid $C_d = 5 \times 10^{-3}$. The time is in days

to the breaking of an elliptical shielded monopole and thus may be subject to the same instability described by Carton and Legras [1994].

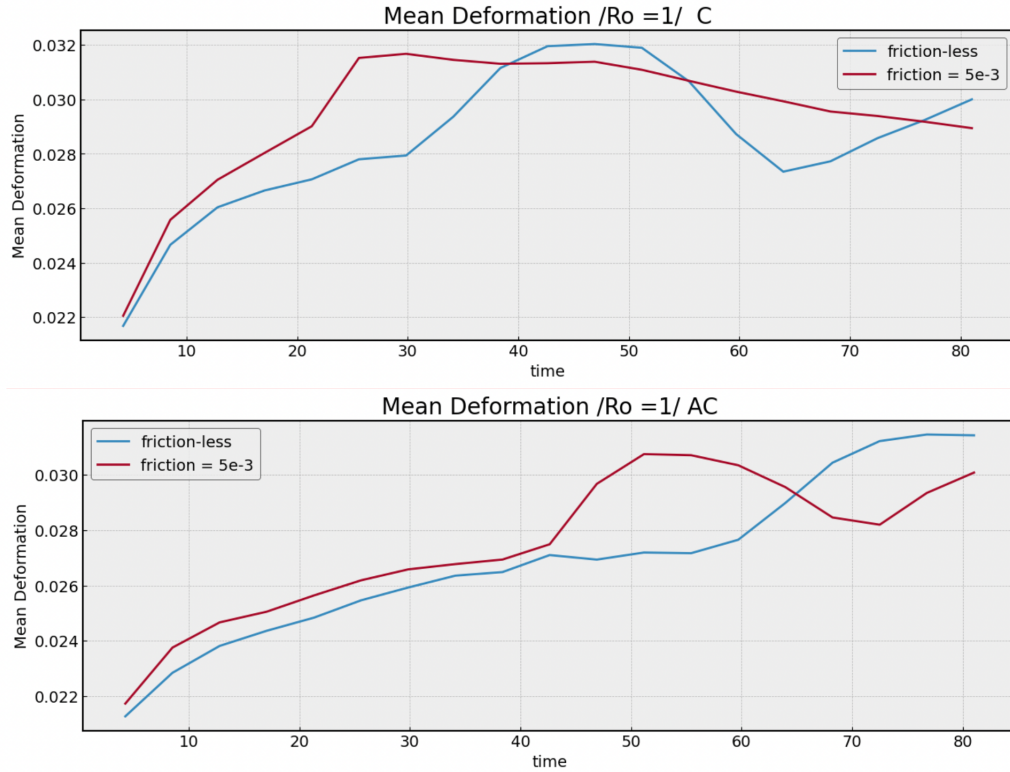


Figure 9: Evolution of the deformation rate ($\sqrt{\text{strain}^2 + \text{shear}^2}$) in time (in days), with friction in red and in ice-free conditions in black, on a cyclonic (top panel), anticyclonic (lower panel) vortex at $Ro = 1$

- The second one is the breaking event for stronger antagonistic influence, as shown in Figure 11. The first steps begins as the merging case but now the peripheral vorticity interacts and forms two poles of opposite-sign of the core. As the cores are too far apart, they are not able to form a coherent structure, and the pair of dipoles formed will mutually repulse and move apart. The most common case is that the pair resulting from the break remains in the form of a dipole pair, but Figure 11 is a case forced by upper lid friction, and thus, as discussed before, the annulus is wrapped around the cores and the two vortices form a pair of shielded monopoles.
- The third case is the peripheral interaction without the merger of the core as illustrated by Figure 12. This case is similar to the previous one but here, the repulsive force exerted by the dipole pair is not strong enough to keep the pair away but is enough to prevent the cores from merging. The pair of monopole shields remain in a stable state in a shape known as a "figure-eight". The distance between the pairs oscillates, attracting and repelling each other. An example of this interaction can be found in the Indian Ocean in the Gulf of Aden region, where an alley of eddies forms.

The corresponding values and time for different experiments are summarized in Table 2. These values indicate no significant differences in merging between the cyclone and anticyclone con-

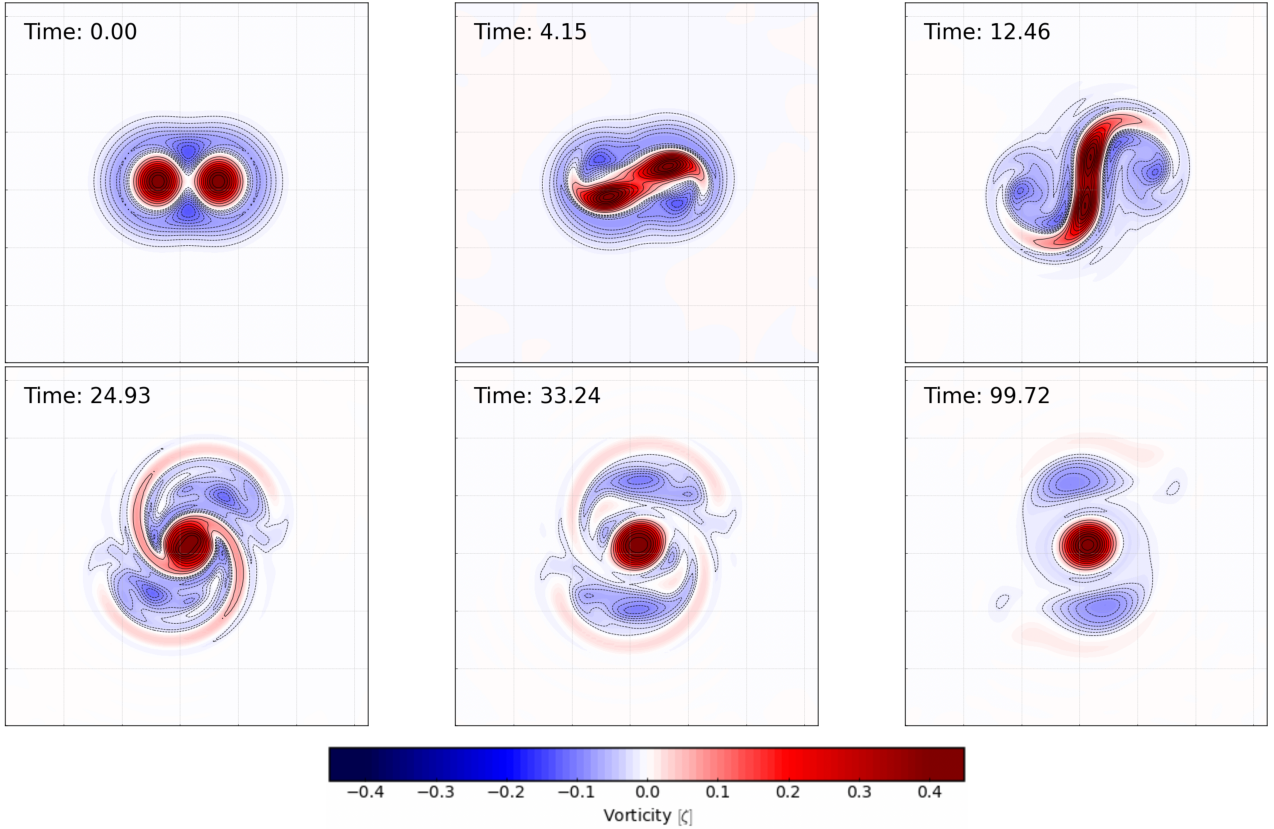


Figure 10: Time-evolution of relative vorticity showing the fusion of two like-sign cyclonic vortices with a steepness $\alpha = 2$ in the lower layer with an $m = 2$ normal-mode (elliptical) perturbation. Both have a Rossby number $Ro = 0.5$ and are distant by $d = 1$, in an idealized Arctic stratification; $Bu = 3.1$. No friction is applied. The time is in days

trary to what was previously suggested by Griffiths and Hopfinger, Valcke and Verron [1996], Carton et al. [2014]. Indeed, here, we found :

- Critical distance without friction for equal relative vorticity : $2 R$
- Critical distance with friction for equal relative vorticity : $1.9 R$

However, according to Carnevale et al. [1991] the reason for this difference could be due to the rigid lid we imposed. Because asymmetries between cyclone and anticyclone would come from the strongest interface deviation for the cyclone.

It also shows friction does not significantly affect the critical merging distance but it does affect the highly slow process.

The critical merging distance we found is between

$$d_c = 1.6 - 2R$$

This value is less than the one found in the literature, which is closer to $d_c = 3.2 - 3.3R$ for barotropic vortices [Dritschel, 1995] and $d_c = 2.5R$ for real Gulf Stream rings [Masina and

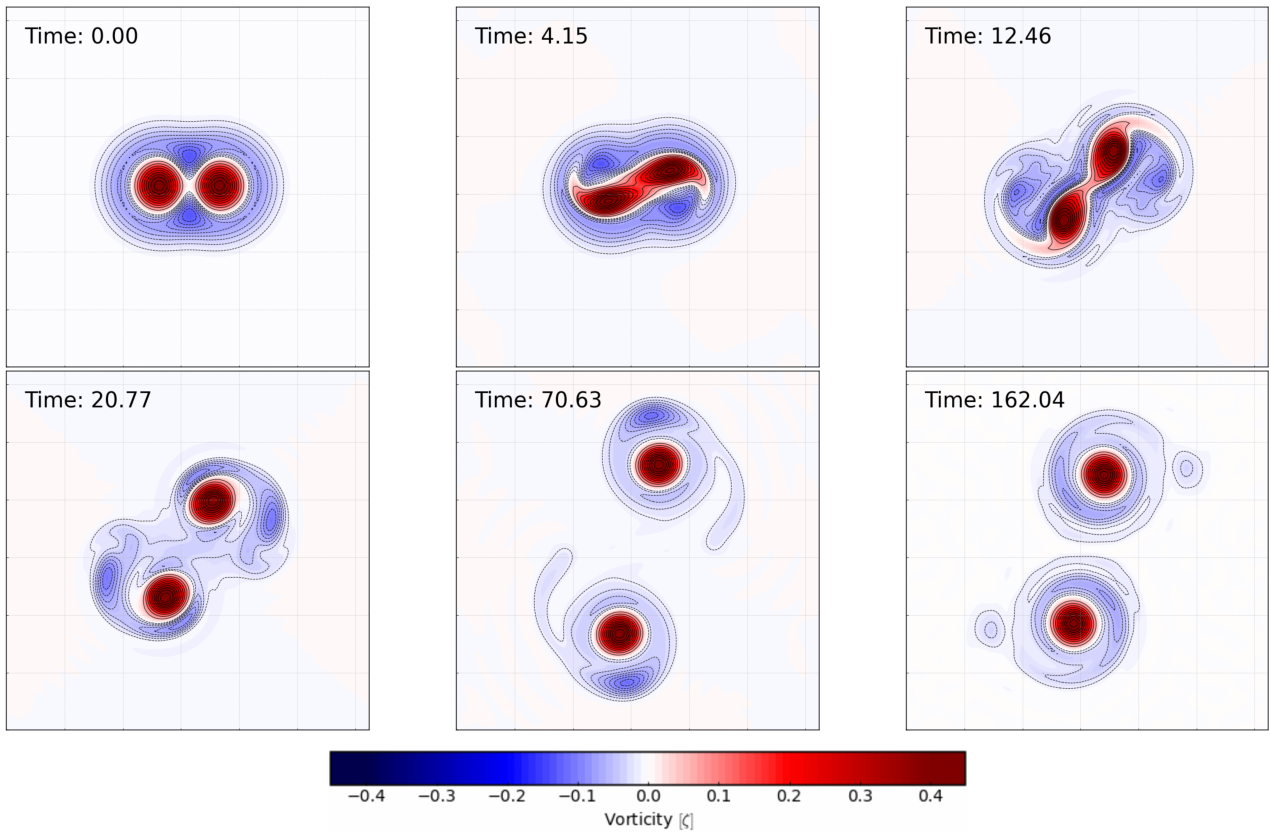


Figure 11: Time-evolution of relative vorticity showing the fusion of two like-sign cyclonic vortex with a steepness $\alpha = 2$ in the lower layer with an $m = 2$ normal-mode (elliptical) perturbation, both have a Rossby number $Ro = 0.5$ and are distant by $d = 1$, in an idealized Arctic stratification; $Bu = 3.1$. Ice–ocean drag coefficient applied on upper lid $C_d = 5 \times 10^{-3}$. The time is in days.

Pinardi, 1991]. The critical merging distance is intrinsically linked to the inner parameter of the vortex [Ciani et al., 2016] and to its environments [Carton et al., 2014]. Particularly, the shielding nature of the vortex plays an antagonist role in the coalescence of vortices [Carton, 1992]. That is the first explanation of why the critical merging distance we found is so small. The second explanation is because we choose to study the Arctic Ocean, where the Rossby deformation is small compared to lower latitudes. Indeed Waugh [1992] shows that great deformation radius is a favorable effect for merging.

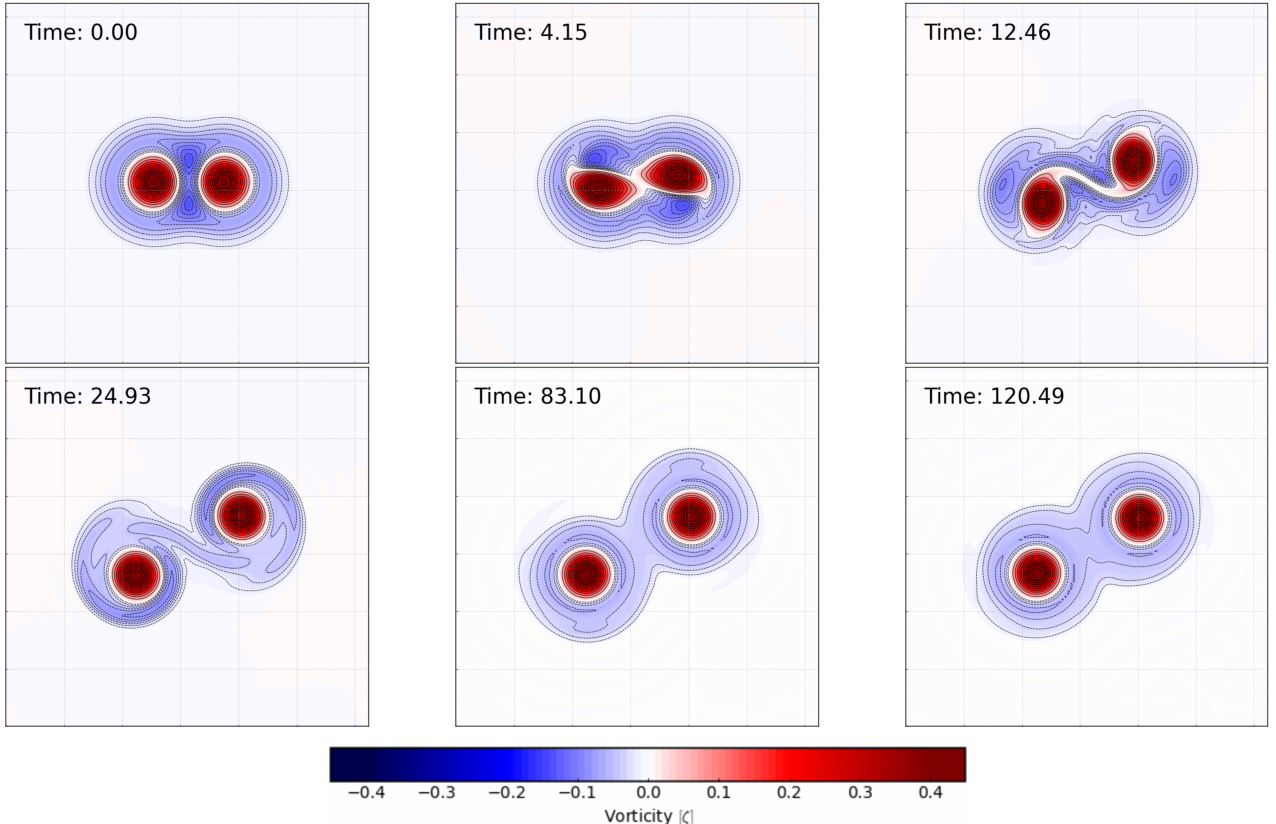


Figure 12: Time-evolution of relative vorticity showing the fusion of two like-sign cyclonic vortex with a steepness $\alpha = 2$ in the lower layer with an $m = 2$ normal-mode (elliptical) perturbation, both have a Rossby number $Ro = 0.5$ and are distant by $d = 1.2$, in an idealized Arctic stratification; $Bu = 3.1$. Ice–ocean drag coefficient applied on upper lid $C_d = 5 \times 10^{-3}$. The time is in days.

		$d = 1.5$		$d = 1.2$		$d = 1$		$d = 0.8$	
		$C_d = 0$	$C_d = 5e^{-3}$	$C_d = 0$	$C_d = 5e^{-3}$	$C_d = 0$	$C_d = 5e^{-3}$	$C_d = 0$	$C_d = 5e^{-3}$
$k = 1$	C	B(2T)-70j	PI(F8)	B(2D)-41j	PI(F8)	M(T)-70j	B(2sMO)-40j	M(T)-30j	M(T)-50j
	AC	B(2T)-66j	PI(F8)	B(2D)-41j	PI(F8)	M(T)-60j	B(2D)-45j	M(T)-30j	M(T)-50j
$k = 0.5$	C	B(2T)-95j	PI(F8)	B(sMo+D)-58j	B(sMo+D)-61j	B(2D)	B(sMo+D)-70j	M(T)-60j	M(T)-120j
	AC	B(sMO+T)-91j	PI(F8)	B(sMo+D)-58j	B(2sMo)-61j	B(2D)-124j	B(sMo+D)-70j	M(T)-60j	M(T)-91j
$k = 0.2$	C	B(T+D)-66j	B(T+D)-66j	B(T+D)-62j	B(sMo+D)-58j	M(sMo)-58j	B(sMo+D)-87j	M(sMo)-45j	M(sMo)-50j
	AC	B(T+D)-66j	B(T+D)-66j	B(sMo+D)-62j	B(sMo+D)-58j	M(sMo)-62j	B(sMo+D)-83j	M(sMo)-45j	M(sMo)-62j

Table 2 : d is the distance separating the center of the core's vortices, k is the ratio of the vorticity of the second vortex of the dipole. The non-linear regime and the final states are given for each case. The non linear regime is given in first by the following symbols: B represents the breaking of the core, M corresponds to the merging of the core, PI is the peripheral interaction without the merger of the core. The final states are classified by the number of coherent structures and their nature: MO is the monopoles, sMo are shielded monopoles, D dipoles, T tripoles, F8 is a "figure-eight" steady state. For example, M (T) corresponds to the merging of the two vortices into a single dipole.

As observed by Ciani et al. [2016], a visual description of the different cases reveals that the merging process induces an elliptical deformation of the core, obviously during the merging but also after. Furthermore, in Figure 13, it appears that friction enhances this deformation, as the red contour is more elliptical than the black one. This confirms the influence of upper lid friction on the core's deformation

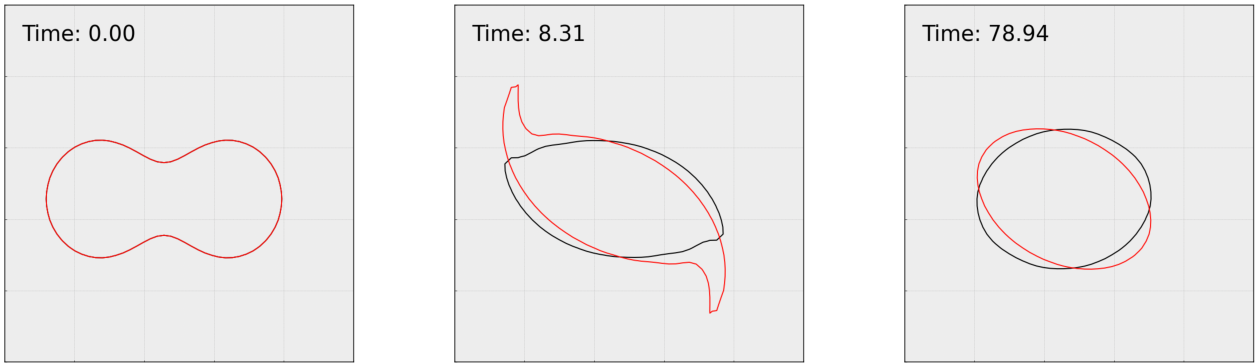


Figure 13: Evolution of the contour the core's vortices during merging, both have a $Ro = 0.5$, and are distant by $d = 1$. Black contour represent ice-free condition, red one represent the case with an upper lid drag of $Cd = 5 \times 10^{-3}$

4.2. Opposite-sign Vortices under upper lid friction

If they are close from each other, two vortices of opposite sign will influence and interact with each other and will propagate in one direction with the cyclone on the left and the anticyclone on the right. We are interested in the effects of friction on this propagation from a kinematic point of view, and its influence on the interaction process. The fundamental parameters that affect the dynamics of two vortices are similar to those for the coalescence process, namely the PV structure, the distance between the core and the environment. However, in contrast to same-sign vortex case, the ratio of vorticity between the vortices of the same size and sign plays a determinant role because it is mostly responsible for the curvature of the trajectory of the dipole. We respectively name the major and the minor vortex the one with the highest and the lowest, in absolute value, relative vorticity.

Figure 14 shows the propagation of a major cyclone interacting with a minor anticyclone. In ice-free condition, in the first time interval, the action of the major cyclone extract the minor anticyclone's cores out of its annulus which itself interacts with the major vortex's annulus forming two patches of vorticity of opposite signs. This major's annulus merges with the minor's core by day 50, forming a dipole that is almost unshielded. The two patches do not form another dipole and do not interact with each other either because they are too distant [Polvani et al., 1989] and thus remain in a steady state for the rest of the simulation. After the coalescence of the minor's core, the two vortices are entangled in such a way that the distance between them does not evolve and the dipole moves as a single coherent structure. The displacement is deflected toward the major's core because its vorticity is larger. The propagation of the dipole

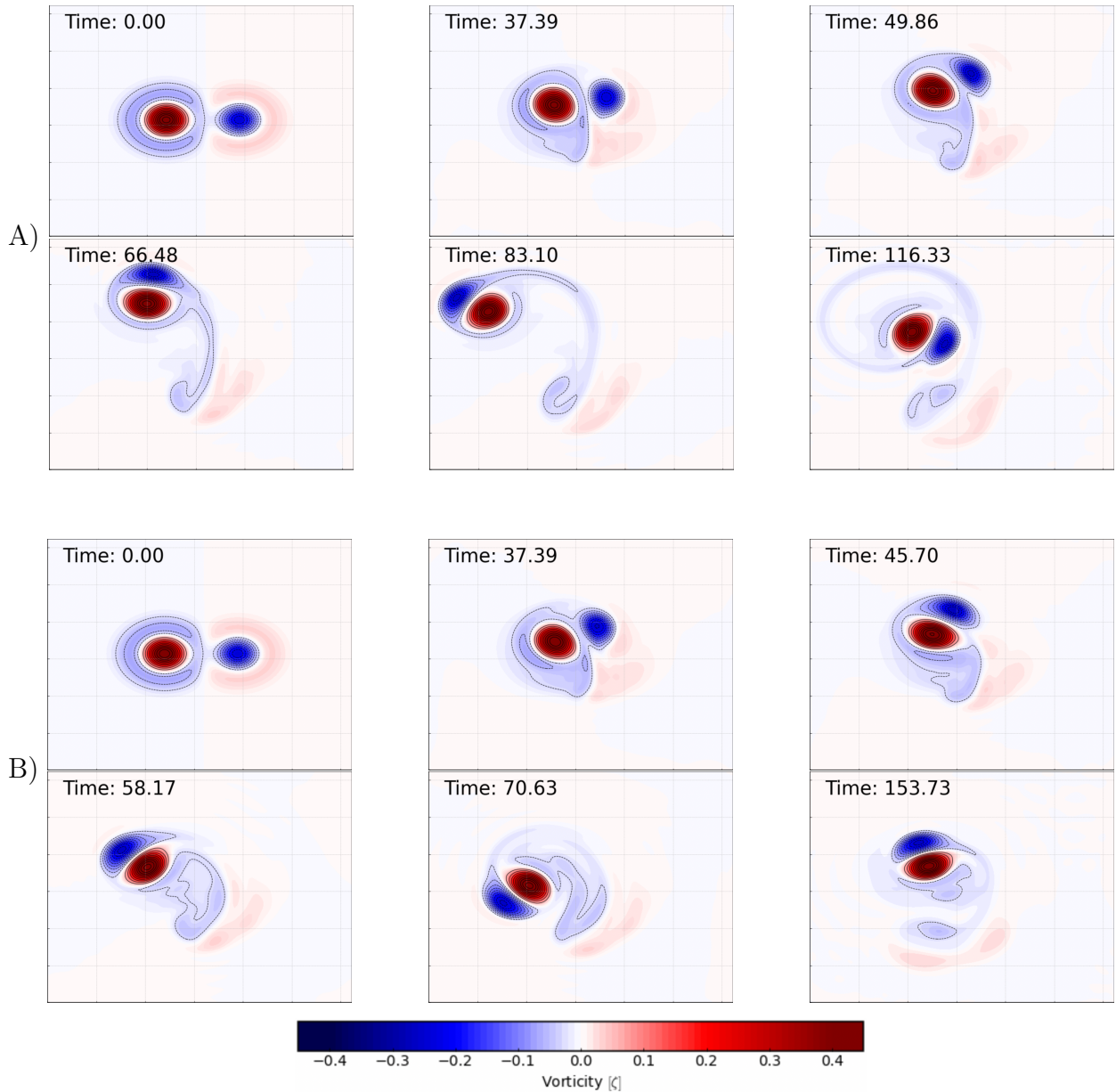


Figure 14: Time-evolution of relative vorticity showing the propagation of two vortexes of opposite sign of a steepness $\alpha = 2$ in the inferior layer, Rossby number $Ro = 1$, in an idealized arctic stratification; $Bu = 3.1$ A): No friction on upper lid, B): Ice–ocean drag coefficient applied on upper lid $C_d = 5.10^{-3}$, The time is in days

is therefore circular and, as the minor vortex is rotated in the opposite direction to its vorticity (that of the major vortex), it is deformed and forms a tail that becomes longer as it moves. It is this loss of vorticity of the minor vortex that leads to a decrease in the influence on the vorticity of the major. As a result, the curvature of the dipole movement is smaller. This explains on day 116 why the dipole's trajectory is not closed and the trajectory takes the form of an inward spiral.

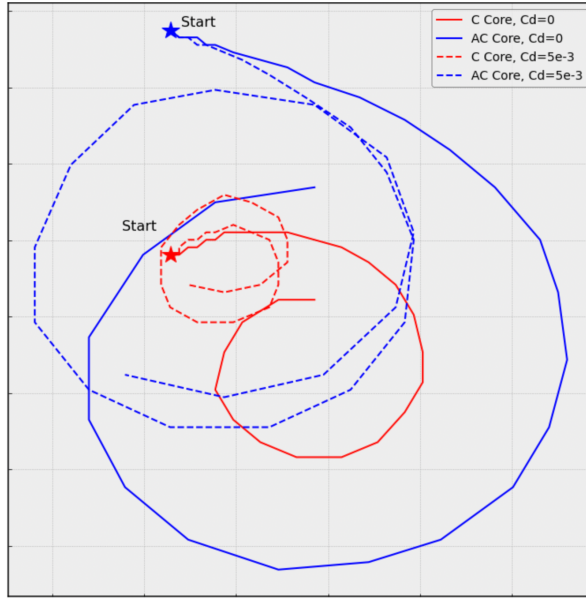


Figure 15: Track of the maximum (minimum) of relative vorticity representing the center of the core of the cyclone (anticyclone) in both friction and frictionless conditions. The Rossby number of the cyclone is $Ro = 0.5$, the absolute vorticity of the anticyclone is half that of the cyclone for the same radius. The distance between the cores is $3 * R$. The track covers 62 days simulated.

The case where the two vortices are forced by sea-ice friction is shown Figure 14 B). The 30 first days are similar to ice-free conditions. On day 50, however, the minor vortex, which is deprived of its screen, only merges with part of the major's annulus, the other part being ejected on the other side. As in the previous case, the cores of the two initial vortices are entangled and follow a circular trajectory. The difference with the ice-free case is that part of the annulus of the major vortex has not merged with the minor core and has not re-formed a screen around the major. Instead, this patch of vorticity, even though it does not form a coherent structure, influences the other two vortices sufficiently to be linked to them. In this way, the two initial cores and the major's screen form a tripolar structure. This is why the trajectory taken by this structure is highly curved. A second dipole is also formed from the ejected patches. At the steady state, this second dipole has the shape of an elliptical structure above a bean one. This shape is consistent with the opposite-signed equilibrium solution for a ratio $k = 0.8$ described by Dritschel [1995].

In this interaction, as discussed before, friction had an antagonistic effect on the coalescence of the minor's core and the major's annulus.

Figure 15 shows the trajectory of the cores for the same experiment. We can see that friction clearly reduces the radius of curvature of the trajectory of the two vortices. We have graphically evaluated this reduction in curvature for different parameters (series of experiments with $k = 0.5$ and $k = 0.2$ for distances d varying between $d = 0.8 - 1.5$) and we obtain a reduction of $19\% \pm 10\%$.

Considering the case of eddy generation described by Manucharyan and Timmermans [2013] and the impact of stress on the propagation of eddies near a front obtained by Brannigan et al. [2017]. Our results show that a dipole is more likely to be trapped, and its displacement will be restrained if it is located under the ice, whereas in ice-free conditions this dipole will have a much larger displacement. This means that the fluxes carried by the dipole will be displaced over greater distances. This implies that the friction of the ice restrains the fluxes and the mass transport due to the propagation of the dipoles.

4.3. Baroclinic Dipole

The presence of friction erases the top layer vortex, whatever its strength within less than a time interval, which corresponds to less than 4 days. This is consistent with the results fund by Ou and Gordon [1986]. After this first time interval and the attenuation of the vortex in the upper layer, the vortex in the deeper layer is preserved and finds itself in the same conditions as in the previous part 3.2.,3.3.,4.1.,4.2..

This result allows us to make the link with the observations. In fact Manucharyan and Timmermans [2013] showed the generation of a dipole made up of a cyclone at the surface and an anticyclone at depth from a front instability and Chao and Shaw [1996] showed the generation of a similar baroclinic dipole from a brine source. These formation processes coupled with the attenuation that our results exhibit are a possible explanation for the predominance of anticyclonic eddies under the Arctic ice observed. However, we have to keep in mind that this observed predominance is not certain, as it may be due to a bias in the observation methods used.

5. Conclusion

We have performed a series of simulations of stability, fusion, and propagation of vortices in an idealized two-and-a-half layers Arctic Ocean using the shallow water equations and pseudo-spectral code.

Our study focused on the dynamics of vortices subjected to friction due to sea ice in an idealized setting. Thanks to this study, we were able to show several results:

- Friction from sea ice does not change the polarity bias of Cyclone /Anticyclone without friction, either in stability or in merging, compared to the no-friction case in shallow water. Anticyclones are more stable and merge more easily than Cyclones in both cases.
- Friction has a localized impact on the core of the vortex, with a negligible impact on the annulus.
- This favors the deformation of the vortex and therefore reduces its stability.
- Friction does not significantly impact the critical merging distance but greatly increases the process duration.
- Friction favors the elliptical deformation of vortices at the end of the merging process.

- Friction reduces the trajectory's curvature radius by a dipole of opposite-sign.

It would therefore be interesting to investigate the robustness of these results in a more realistic high-resolution setting and give a more qualitative correlation between sea-ice conditions and the evolution of vortices.

We have therefore been able to show in this work that friction has a real impact on the dynamics of vortices, which is antagonistic to their lifetime and seems to undermine the process of reverse energy cascade. In the context of the Arctic Ocean, this impact has several implications. As mentioned in the introduction, the ice cover is tending to shrink from year to year and will even disappear during the summer months in the coming decades [Meier and Stroeve, 2022]. The role of eddies in this region will therefore evolve, in the formation of water masses and in the large-scale dynamics of the Arctic, in the same way as their role in the dynamics of the Beaufort gyre Doddridge et al. [2019]. Thus, as we have seen, sea ice friction has important implications for the dynamics and thermodynamics of the Arctic Ocean.

It is necessary to bear in mind certain limitations of our study:

- The model we choose is highly idealized and therefore, the vortex is always placed in the second layer which is below the peak of stratification.
- We have chosen to implement the perturbation in mode two, as the non-linear code used in this analysis requires a perturbation in angular mode. In all rigor, the stability study should implement the normal mode of perturbation which will be different for each configuration. We do not solve the barotropic mode and therefore an analysis with a different model is required to determine the impact of friction on the barotropic mode.
- The merging experiments were designed to study the influence of friction on this process. Obviously, in an open ocean, two vortices will not spontaneously be closer to the critical merging distance without external forcing or the annulus would have interacted upstream, redistributed opposite-sign vorticity, and prevented coalescence. The merging process under sea ice, which should be investigated, requires a more realistic experiment and a high-resolution model.

In light of the results from this work, it would be interesting to study the impact of sea ice friction on the deformation field and also its impact on ageostrophic movement, in particular the filamentation of eddies under the sea ice.

Appendix A: Linear stability in a 2 + 1/2 layer Shallow-Water subjected to upper lid frictional forcing

The nomenclature of the layers follows the diagram in Figure 1, layer 1 is the layer in contact with the sea ice, layer 2 is the intermedial layer, layer 3 is a layer of infinite depth at rest.

Bottom infinite layer at rest

$$\begin{aligned} p_2 &= p_1 + \rho_0 g_1 \eta_1, & p_3 &= p_2 + \rho_0 g_2 \eta_2 \\ \nabla p_3 = 0 &\Rightarrow \frac{\nabla p_1}{\rho_0} = -g_1 \nabla \eta_1 - g_2 \nabla \eta_2; & \frac{\nabla p_2}{\rho_0} &= -g_2 \nabla \eta_2 \end{aligned}$$

Layer 1:

U, V are the radial and azimuthal speeds respectively

$$\left[\partial_t + U_1 \partial_r + \frac{V_1}{r} \partial_\theta \right] U_1 - \frac{V_1^2}{r} - V_1 f_0 = -g_1 \partial_r \eta_1 - g_2 \partial_r \eta_2 - C_f U_1 \quad (8)$$

$$\left[\partial_t + U_1 \partial_r + \frac{V_1}{r} \partial_\theta \right] V_1 + \frac{U_1 V_1}{r} + U_1 f_0 = -\frac{g_1}{r} \partial_\theta \eta_1 - \frac{g_2}{r} \partial_\theta \eta_2 - C_f V_1 \quad (9)$$

$$\left[\partial_t + U_1 \partial_r + \frac{V_1}{r} \partial_\theta \right] (H_1 - \eta_1) + \frac{(H_1 - \eta_1)}{r} [\partial_r(rU_1) + \partial_\theta V_1] = 0 \quad (10)$$

Layer 2:

$$\left[\partial_t + U_2 \partial_r + \frac{V_2}{r} \partial_\theta \right] U_2 - \frac{V_2^2}{r} - V_2 f_0 = -g_2 \partial_r \eta_2 \quad (11)$$

$$\left[\partial_t + U_2 \partial_r + \frac{V_2}{r} \partial_\theta \right] V_2 + \frac{U_2 V_2}{r} + U_2 f_0 = -\frac{g_2}{r} \partial_\theta \eta_2 \quad (12)$$

$$\left[\partial_t + U_2 \partial_r + \frac{V_2}{r} \partial_\theta \right] (H_2 - \eta_2) + \frac{(H_2 - \eta_2)}{r} [\partial_r(rU_2) + \partial_\theta V_2] = 0 \quad (13)$$

Mean flow : Circular vortices

$$v(r) = v_0 r e^{-r^\alpha}$$

Cyclogeostrophic balance:

$$\frac{v^2(r)}{r} + f_0 v(r) = g \frac{d\eta}{dr} \quad (14)$$

Perturbation of the mean flow

$$(U_i, V_i, \eta_i) = \left(\bar{u}_i + u'_i(r) e^{il(\theta-ct)}, \bar{v}_i + v'_i(r) e^{il(\theta-ct)}, \bar{\eta}_i + \eta'_i(r) e^{il(\theta-ct)} \right)$$

Linearised equations in normal mode

Exponentials are not noted

Layer 1:

$$\left[\partial_t + \frac{\bar{v}_1}{r} \partial_\theta \right] u'_1 - (2\frac{\bar{v}_1}{r} + f_0) v'_1 = -g_1 \partial_r \eta'_1 - g_2 \partial_r \eta'_2 - C_f u'_1 \quad (15)$$

$$\left[\partial_t + \frac{\bar{v}_1}{r} \partial_\theta \right] v'_1 + (\bar{v}_1 r + f_0) u'_1 = -\frac{g_1}{r} \partial_\theta \eta'_1 - \frac{g_2}{r} \partial_\theta \eta'_2 - C_f v'_1 \quad (16)$$

$$\left[\partial_t + \frac{\bar{v}_1}{r} \partial_\theta \right] (H_1 - \eta'_1) + \frac{(H_1 - \bar{\eta}_1)}{r} [\partial_r(ru_1) + \partial_\theta v_1] = 0 \quad (17)$$

Layer 2:

$$\left[\partial_t + \frac{\bar{v}_2}{r} \partial_\theta \right] u'_2 - (2\frac{\bar{v}_2}{r} + f_0) v'_2 = -g_2 \partial_r \eta'_2 \quad (18)$$

$$\left[\partial_t + \frac{\bar{v}_2}{r} \partial_\theta \right] v'_2 + (\bar{v}_2 r + f_0) u'_2 = -\frac{g_2}{r} \partial_\theta \eta'_2 \quad (19)$$

$$\left[\partial_t + \frac{\bar{v}_2}{r} \partial_\theta \right] (H_2 - \eta'_2) + \frac{(H_2 - \bar{\eta}_2)}{r} [\partial_r(ru_2) + \partial_\theta v_2] = 0 \quad (20)$$

Normal mode linearized equations in Fourier space

Layer 1:

$$\left[Ro \left(il \frac{\bar{v}_1}{r} \right) + Ek \right] u'_1 - \left(2Ro \frac{\bar{v}_1}{r} + 1 \right) v'_1 = -\frac{Bu_1}{Ro} \frac{d}{dr} \eta'_1 - \frac{Bu_2}{Ro} \frac{d}{dr} \eta'_2 \quad (21)$$

$$\left[Ro \left(il \frac{\bar{v}_1}{r} \right) + Ek \right] v'_1 + \left(Ro \frac{\bar{v}_1}{r} + 1 \right) u'_1 = -\frac{il}{r} \frac{Bu_1}{Ro} \eta'_1 - \frac{il}{r} \frac{Bu_2}{Ro} \frac{d}{dr} \eta'_2 \quad (22)$$

$$il \frac{\bar{v}_1}{r} (-\eta'_1) + \frac{(H_1 - \bar{\eta}_1)}{r} \left[\frac{d}{dr} (ru'_1) + ilv'_1 \right] = 0 \quad (23)$$

Layer 2:

$$Ro \left(il \frac{\bar{v}_2}{r} \right) u'_2 - \left(2Ro \frac{\bar{v}_2}{r} + 1 \right) v'_2 = -\frac{Bu_2}{Ro} \frac{d}{dr} \eta'_2 \quad (24)$$

$$Ro \left(il \frac{\bar{v}_2}{r} \right) v'_2 + \left(Ro \frac{\bar{v}_2}{r} + 1 \right) u'_2 = -\frac{il}{r} \frac{Bu_2}{Ro} \frac{d}{dr} \eta'_2 \quad (25)$$

$$il \frac{\bar{v}_2}{r} (-\eta'_2) + \frac{(H_2 - \bar{\eta}_2)}{r} \left[\frac{d}{dr} (ru'_2) + ilv'_2 \right] = 0 \quad (26)$$

Bibliography

- Jean-Michel Baey and Xavier Carton. Vortex multipoles in two-layer rotating shallow-water flows. *Journal of Fluid Mechanics*, 460:151–175, June 2002. ISSN 0022-1120, 1469-7645. doi: 10.1017/S0022112002008170. URL https://www.cambridge.org/core/product/identifier/S0022112002008170/type/journal_article.
- Liam Brannigan, Helen Johnson, Camille Lique, Jonas Nylander, and Johan Nilsson. Generation of Subsurface Anticyclones at Arctic Surface Fronts due to a Surface Stress. *Journal of Physical Oceanography*, 47(11):2653–2671, November 2017. ISSN 0022-3670, 1520-0485. doi: 10.1175/JPO-D-17-0022.1. URL <https://journals.ametsoc.org/view/journals/phoc/47/11/jpo-d-17-0022.1.xml>.
- G. F. Carnevale, P. Cavazza, P. Orlandi, and R. Purini. An explanation for anomalous vortex merger in rotating-tank experiments. *Physics of Fluids A: Fluid Dynamics*, 3(5):1411–1415, May 1991. ISSN 0899-8213. doi: 10.1063/1.858019. URL <https://doi.org/10.1063/1.858019>.
- J. R. Carpenter and M.-L. Timmermans. Deep mesoscale eddies in the Canada Basin, Arctic Ocean. *Geophysical Research Letters*, 39(20):2012GL053025, October 2012. ISSN 0094-8276, 1944-8007. doi: 10.1029/2012GL053025. URL <https://onlinelibrary.wiley.com/doi/abs/10.1029/2012GL053025>.
- X. J. Carton. On the Merger of Shielded Vortices. *Europhysics Letters*, 18(8):697, April 1992. ISSN 0295-5075. doi: 10.1209/0295-5075/18/8/006. URL <https://dx.doi.org/10.1209/0295-5075/18/8/006>.
- Xavier Carton. Hydrodynamical Modeling Of Oceanic Vortices. *Surveys in Geophysics*, 22(3):179–263, 2001. ISSN 01693298. doi: 10.1023/A:1013779219578. URL <http://link.springer.com/10.1023/A:1013779219578>.
- Xavier Carton and Bernard Legras. The life-cycle of tripoles in two-dimensional incompressible flows. *Journal of Fluid Mechanics*, 267:53–82, May 1994. ISSN 0022-1120, 1469-7645. doi: 10.1017/S0022112094001114. URL https://www.cambridge.org/core/product/identifier/S0022112094001114/type/journal_article.
- Xavier Carton, Mikhail Sokolovskiy, Claire Menesguen, Ana Aguiar, and Thomas Meunier. Vortex stability in a multi-layer quasi-geostrophic model: application to Mediterranean Water eddies. *Fluid Dynamics Research*, 46(6):061401, December 2014. ISSN 0169-5983. doi: 10.1088/0169-5983/46/6/061401. URL <https://www.webofscience.com/wos/woscc/summary/9e59dc52-4cba-414d-be89-d06c97bce8b5-24d80ab3/relevance/2>. Place: Bristol Publisher: Iop Publishing Ltd WOS:000345913500002.
- X.J. Carton and J.C. Mcwilliams. Barotropic and Baroclinic Instabilities of Axisymmetric Vortices in a Quasi-geostrophic Model. *Elsevier Oceanography Series*, 50:225–244, 1989. doi: 10.1016/S0422-9894(08)70188-0. URL <https://linkinghub.elsevier.com/retrieve/pii/S0422989408701880>.
- Shenn-Yu Chao and Ping-Tung Shaw. Initialization, Asymmetry, and Spindown of Arctic Eddies. *Journal of Physical Oceanography*, 26(10):2076–2092, October 1996. ISSN 0022-3670, 1520-0485. doi: 10.1175/1520-0485(1996)026<2076:IAASOA>2.0.CO;2. URL https://journals.ametsoc.org/view/journals/phoc/26/10/1520-0485_1996_026_2076_iaaso_2_0_co_2.xml. Publisher: American Meteorological Society Section: Journal of Physical Oceanography.
- Daniele Ciani, Xavier Carton, and Jacques Verron. On the merger of subsurface isolated vortices. *Geophysical and Astrophysical Fluid Dynamics*, 110(1):23–49, January 2016. ISSN 0309-1929. doi: 10.1080/03091929.2015.1135430. URL <https://www.webofscience.com/wos/woscc/summary/9e59dc52-4cba-414d-be89-d06c97bce8b5-24d80ab3/relevance/2>. Place: Abingdon Publisher: Taylor & Francis Ltd WOS:000371645800002.
- Sylvia T. Cole, Mary-Louise Timmermans, John M. Toole, Richard A. Krishfield, and Fredrik T. Thwaites. Ekman Veering, Internal Waves, and Turbulence Observed under Arctic Sea Ice. *Journal of Physical Oceanography*, 44(5):1306–1328, May 2014. ISSN 0022-3670, 1520-0485. doi: 10.1175/JPO-D-12-0191.1. URL <http://journals.ametsoc.org/doi/10.1175/JPO-D-12-0191.1>.

Eric A. D'Asaro. Observations of small eddies in the Beaufort Sea. *Journal of Geophysical Research: Oceans*, 93(C6):6669–6684, 1988. ISSN 2156-2202. doi: 10.1029/JC093iC06p06669. URL <https://onlinelibrary.wiley.com/doi/abs/10.1029/JC093iC06p06669>. eprint: <https://onlinelibrary.wiley.com/doi/pdf/10.1029/JC093iC06p06669>.

Edward W. Doddridge, Gianluca Meneghelli, John Marshall, Jeffery Scott, and Camille Lique. A Three-Way Balance in the Beaufort Gyre: The Ice-Ocean Governor, Wind Stress, and Eddy Diffusivity. *Journal of Geophysical Research: Oceans*, 124(5):3107–3124, 2019. ISSN 2169-9291. doi: 10.1029/2018JC014897. URL <https://onlinelibrary.wiley.com/doi/abs/10.1029/2018JC014897>. eprint: <https://onlinelibrary.wiley.com/doi/pdf/10.1029/2018JC014897>.

David G. Dritschel. A general theory for two-dimensional vortex interactions. *Journal of Fluid Mechanics*, 293:269–303, June 1995. ISSN 1469-7645, 0022-1120. doi: 10.1017/S0022112095001716. URL <https://www.cambridge.org/core/journals/journal-of-fluid-mechanics/article/abs/general-theory-for-twodimensional-vortex-interactions/A3E366852F569474CB7F7FF3027EB1C3>. Publisher: Cambridge University Press.

Glenn R. Flierl. On the instability of geostrophic vortices. *Journal of Fluid Mechanics*, 197:349–388, December 1988. ISSN 0022-1120, 1469-7645. doi: 10.1017/S0022112088003283. URL https://www.cambridge.org/core/product/identifier/S0022112088003283/type/journal_article.

R W Griffiths and E J Hopfinger. Coalescing of geostrophic vortices.

James R. Holton. *An introduction to dynamic meteorology*. Number v. 88 in International geophysics series. Elsevier Academic Press, Burlington, MA, 4th ed edition, 2004. ISBN 978-0-12-354015-7 978-0-12-354016-4. OCLC: 54400282.

O. M. Johannessen, J. A. Johannessen, E. Svendsen, R. A. Shuchman, W. J. Campbell, and E. Josberger. Ice-Edge Eddies in the Fram Strait Marginal Ice Zone. *Science*, 236(4800):427–429, April 1987. ISSN 0036-8075, 1095-9203. doi: 10.1126/science.236.4800.427. URL <https://www.science.org/doi/10.1126/science.236.4800.427>.

T. O. Manley and Kenneth Hunkins. Mesoscale eddies of the Arctic Ocean. *Journal of Geophysical Research: Oceans*, 90(C3):4911–4930, 1985. ISSN 2156-2202. doi: 10.1029/JC090iC03p04911. URL <https://onlinelibrary.wiley.com/doi/abs/10.1029/JC090iC03p04911>. eprint: <https://onlinelibrary.wiley.com/doi/pdf/10.1029/JC090iC03p04911>.

Georgy E. Manucharyan and Mary-Louise Timmermans. Generation and Separation of Mesoscale Eddies from Surface Ocean Fronts. *Journal of Physical Oceanography*, 43(12):2545–2562, December 2013. ISSN 0022-3670, 1520-0485. doi: 10.1175/JPO-D-13-094.1. URL <https://journals.ametsoc.org/view/journals/phoc/43/12/jpo-d-13-094.1.xml>. Publisher: American Meteorological Society Section: Journal of Physical Oceanography.

Charlotte L. J. Marcinko, Adrian P. Martin, and John T. Allen. Characterizing horizontal variability and energy spectra in the Arctic Ocean halocline. *Journal of Geophysical Research: Oceans*, 120(1):436–450, 2015. ISSN 2169-9291. doi: 10.1002/2014JC010381. URL <https://onlinelibrary.wiley.com/doi/abs/10.1002/2014JC010381>. eprint: <https://onlinelibrary.wiley.com/doi/pdf/10.1002/2014JC010381>.

S. Masina and N. Pinardi. Merging of barotropic symmetric vortices. A case study for gulf stream rings. *Il Nuovo Cimento C*, 14(6):539–553, November 1991. ISSN 0390-5551. doi: 10.1007/BF02507382. URL <https://doi.org/10.1007/BF02507382>.

Matthew R. Mazloff, Patrick Heimbach, and Carl Wunsch. An Eddy-Permitting Southern Ocean State Estimate. *Journal of Physical Oceanography*, 40(5):880–899, May 2010. ISSN 1520-0485, 0022-3670. doi: 10.1175/2009JPO4236.1. URL <http://journals.ametsoc.org/doi/10.1175/2009JPO4236.1>.

Walter Meier and Julianne Stroeve. An Updated Assessment of the Changing Arctic Sea Ice Cover. *Oceanography*, 2022. ISSN 10428275. doi: 10.5670/oceanog.2022.114. URL <https://tos.org/oceanography/article/an-updated-assessment-of-the-changing-arctic-sea-ice-cover>.

Jean A. Mensa and M. L. Timmermans. Characterizing the seasonal cycle of upper-ocean flows under multi-year sea ice. *Ocean Modelling*, 113:115–130, May 2017. ISSN 1463-5003. doi: 10.1016/j.ocemod.2017.03.009. URL <https://www.sciencedirect.com/science/article/pii/S1463500317300409>.

J. L. Newton, K. Aagaard, and L. K. Coachman. Baroclinic eddies in the Arctic Ocean. *Deep Sea Research and Oceanographic Abstracts*, 21(9):707–719, September 1974. ISSN 0011-7471. doi: 10.1016/0011-7471(74)90078-3. URL <https://www.sciencedirect.com/science/article/pii/0011747174900783>.

- Hw Ou and Al Gordon. Spin-down of Baroclinic Eddies Under Sea Ice. *Journal of Geophysical Research-Oceans*, 91(C6):7623–7630, June 1986. doi: 10.1029/JC091iC06p07623. URL <https://www.webofscience.com/wos/woscc/full-record/WOS:A1986C869200005>. Place: Washington Publisher: Amer Geophysical Union WOS:A1986C869200005.
- C. H. Pease, S. A. Salo, and J. E. Overland. Drag measurements for first-year sea ice over a shallow sea. *Journal of Geophysical Research*, 88(C5):2853, 1983. ISSN 0148-0227. doi: 10.1029/JC088iC05p02853. URL <http://doi.wiley.com/10.1029/JC088iC05p02853>.
- Joseph Pedlosky. *Geophysical Fluid Dynamics*. Springer, New York, NY, 1987. ISBN 978-0-387-96387-7 978-1-4612-4650-3. doi: 10.1007/978-1-4612-4650-3. URL <http://link.springer.com/10.1007/978-1-4612-4650-3>.
- Andrey Pnyushkov, Igor V. Polyakov, Laurie Padman, and An T. Nguyen. Structure and dynamics of mesoscale eddies over the Laptev Sea continental slope in the Arctic Ocean. *Ocean Science*, 14(5):1329–1347, October 2018. ISSN 1812-0792. doi: 10.5194/os-14-1329-2018. URL <https://os.copernicus.org/articles/14/1329/2018/>.
- L. M. Polvani, N. J. Zabusky, and G. R. Flierl. Two-layer geostrophic vortex dynamics. Part 1. Upper-layer V-states and merger. *Journal of Fluid Mechanics*, 205(-1):215, August 1989. ISSN 0022-1120, 1469-7645. doi: 10.1017/S0022112089002016. URL http://www.journals.cambridge.org/abstract_S0022112089002016.
- P. Ripa. General stability conditions for a multi-layer model. *Journal of Fluid Mechanics*, 222(-1):119, January 1991. ISSN 0022-1120, 1469-7645. doi: 10.1017/S0022112091001027. URL http://www.journals.cambridge.org/abstract_S0022112091001027.
- Erica Rosenblum, Julianne Stroeve, Sarah T. Gille, Camille Lique, Robert Fajber, L. Bruno Tremblay, Ryan Galley, Thiago Loureiro, David G. Barber, and Jennifer V. Lukovich. Freshwater Input and Vertical Mixing in the Canada Basin's Seasonal Halocline: 1975 versus 2006–12. *Journal of Physical Oceanography*, 52(7):1383–1396, July 2022. ISSN 0022-3670, 1520-0485. doi: 10.1175/JPO-D-21-0116.1. URL <https://journals.ametsoc.org/view/journals/phoc/52/7/JPO-D-21-0116.1.xml>. Publisher: American Meteorological Society Section: Journal of Physical Oceanography.
- Michael A. Spall. Frontogenesis, subduction, and cross-front exchange at upper ocean fronts. *Journal of Geophysical Research*, 100(C2):2543, 1995. ISSN 0148-0227. doi: 10.1029/94JC02860. URL <http://doi.wiley.com/10.1029/94JC02860>.
- M.-L. Timmermans, J. Toole, A. Proshutinsky, R. Krishfield, and A. Plueddemann. Eddies in the Canada Basin, Arctic Ocean, Observed from Ice-Tethered Profilers. *Journal of Physical Oceanography*, 38(1):133–145, January 2008. ISSN 0022-3670, 1520-0485. doi: 10.1175/2007JPO3782.1. URL <https://journals.ametsoc.org/view/journals/phoc/38/1/2007jpo3782.1.xml>. Publisher: American Meteorological Society Section: Journal of Physical Oceanography.
- S. Valcke and J. Verron. Cyclone—anticyclone asymmetry in the merging process. *Dynamics of Atmospheres and Oceans*, 24(1-4):227–236, January 1996. ISSN 03770265. doi: 10.1016/0377-0265(95)00450-5. URL <https://linkinghub.elsevier.com/retrieve/pii/0377026595004505>.
- S. Valcke and J. Verron. Interactions of Baroclinic Isolated Vortices: The Dominant Effect of Shielding. *Journal of Physical Oceanography*, 27(4):524–541, April 1997. ISSN 0022-3670, 1520-0485. doi: 10.1175/1520-0485(1997)027<0524:IOBIVT>2.0.CO;2. URL https://journals.ametsoc.org/view/journals/phoc/27/4/1520-0485_1997_027_0524_iobivt_2.0.co_2.xml. Publisher: American Meteorological Society Section: Journal of Physical Oceanography.
- J. Verron and S. Valcke. Scale-dependent merging of baroclinic vortices. *Journal of Fluid Mechanics*, 264:81–106, April 1994. ISSN 0022-1120, 1469-7645. doi: 10.1017/S0022112094000595. URL https://www.cambridge.org/core/product/identifier/S0022112094000595/type/journal_article.
- Wilken-Jon von Appen, Till Baumann, Markus Janout, Nikolay Koldunov, Yueng-Djern Lenn, Robert Pickart, Robert Scott, and Qiang Wang. Eddies and the Distribution of Eddy Kinetic Energy in the Arctic Ocean. *Oceanography (Washington D.C.)*, 35, April 2022. doi: 10.5670/oceanog.2022.122.
- Darryn W. Waugh. The efficiency of symmetric vortex merger. *Physics of Fluids A: Fluid Dynamics*, 4(8):1745–1758, August 1992. ISSN 0899-8213. doi: 10.1063/1.858395. URL <https://doi.org/10.1063/1.858395>.
- Mengnan Zhao and Mary-Louise Timmermans. Vertical scales and dynamics of eddies in the Arctic Ocean's Canada Basin. *Journal of Geophysical Research: Oceans*, 120(12):8195–8209, December 2015. ISSN 2169-9275, 2169-9291. doi: 10.1002/2015JC011251. URL <https://onlinelibrary.wiley.com/doi/10.1002/2015JC011251>.

Mengnan Zhao, Mary-Louise Timmermans, Sylvia Cole, Richard Krishfield, Andrey Proshutinsky, and John Toole. Characterizing the eddy field in the Arctic Ocean halocline. *Journal of Geophysical Research: Oceans*, 119(12):8800–8817, December 2014. ISSN 21699275. doi: 10.1002/2014JC010488. URL <http://doi.wiley.com/10.1002/2014JC010488>.

Mengnan Zhao, Mary-Louise Timmermans, Sylvia Cole, Richard Krishfield, and John Toole. Evolution of the eddy field in the Arctic Ocean’s Canada Basin, 2005–2015. *Geophysical Research Letters*, 43(15):8106–8114, 2016. ISSN 1944-8007. doi: 10.1002/2016GL069671. URL <https://onlinelibrary.wiley.com/doi/abs/10.1002/2016GL069671>. eprint: <https://onlinelibrary.wiley.com/doi/pdf/10.1002/2016GL069671>.